International Journal of Biological Macromolecules 273 (2024) 132892

Contents lists available at ScienceDirect

International Journal of Biological Macromolecules

journal homepage: www.elsevier.com/locate/ijbiomac

Fine-tuning pH sensor H98 by remote essential residues in the hydrogen-bond network of mTASK-3

Xueming Fan [a,b,1], Yifei Ye [b,c,1], Aakash Saha [d], Li Peng [b], Chinmai Pindi [d], Qi Wang [b,c], Linghui Yang [b], Jin Liu [b,c], Xiangdong Tang [e,f,g], Giulia Palermo [d], Jiayu Liao [d,h], Tingting Xu [i], Yongzhi Lu [j,*], Guizhi Du [b,c,**]

[a] Department of Pain Management, West China Hospital of Sichuan University, Chengdu, Sichuan 610041, China
[b] Laboratory of Anesthesia and Critical Care Medicine, National-Local Joint Engineering Research Centre of Translational Medicine of Anesthesiology, West China Hospital of Sichuan University, Chengdu, Sichuan 610000, China
[c] Department of Anesthesiology, West China Hospital of Sichuan University, Chengdu, Sichuan 610041, China
[d] Department of Bioengineering, University of California Riverside, 900 University Avenue, Riverside, CA 92521, United States
[e] Sleep Medicine Center, West China Hospital of Sichuan University, Chengdu, Sichuan 610041, China
[f] Mental Health Center, West China Hospital of Sichuan University, Chengdu, Sichuan 610041, China
[g] State Key Laboratory of Biotherapy, West China Hospital of Sichuan University, Chengdu, Sichuan 610041, China
[h] Huaxi-Cal Research Center for Predictive Intervention Medicine, West China Hospital of Sichuan University, Chengdu, Sichuan 610000, China
[i] Guangdong Provincial Key Laboratory of Biocomputing, Guangzhou Institutes of Biomedicine and Health, Chinese Academy of Sciences, Guangzhou, Guangdong 510530, China
[j] Guangzhou National Laboratory, Guangzhou International Bio Island, Guangzhou, Guangdong 510005, China

ARTICLE INFO

Keywords:
pH sensitivity
Hydrogen-bond network
Remote tuning
H98
S31
mTASK-3

ABSTRACT

TASK-3 generates a background K^+ conductance which when inhibited by acidification depolarizes membrane potential and increases cell excitability. These channels sense pH by protonation of histidine residue H98, but recent evidence revealed that several other amino acid residues also contribute to TASK-3 pH sensitivity, suggesting that the pH sensitivity is determined by an intermolecular network. Here we use electrophysiology and molecular modeling to characterize the nature and requisite role(s) of multiple amino acids in pH sensing by TASK-3. Our results suggest that the pH sensor H98 and consequently pH sensitivity is influenced by remote amino acids that function as a hydrogen-bonding network to modulate ionic conductivity. Among the residues in the network, E30 and K79 are the most important for passing external signals near residue S31 to H98. The hydrogen-bond network plays a key role in selectivity or pH sensing in mTASK-3, and E30 and S31 in the network can modulate the conductive properties (E30) or reverse the pH sensitivity and selectivity of the channel (S31). Molecular dynamics simulations and $pK_{1/2}$ calculation revealed that double mutants involving H98 + S31 primarily regulate the structure stability of the pore selectivity filter and pore loop regions, further strengthen the stability of the cradle suspension system, and alter the ionization state of E30 and K79, thereby preventing pore conformational change that normally occurs in response to varying extracellular pH. These results demonstrate that crucial residues in the hydrogen-bond network can remotely tune the pH sensing of mTASK-3 and may be a potential allosteric regulatory site for therapeutic molecule development.

1. Introduction

TWIK-related acid-sensitive K channels (TASK-1, K2P3.1; TASK-3, K2P9.1) are members of the two-pore-domain family of potassium (K2P) channels which generate a pH-sensitive background K^+ conductance that contributes to membrane potential and the regulation of cell

* Correspondence to: Yongzhi Lu, Guangzhou National Laboratory, Guangzhou International Bio Island, Guangzhou, Guangdong 510005, China.
** Correspondence to: Guizhi Du, Laboratory of Anesthesia and Critical Care Medicine, National-Local Joint Engineering Research Centre of Translational Medicine of Anesthesiology, West China Hospital of Sichuan University, Chengdu, Sichuan 610041, China.
E-mail addresses: lu_yongzhi@gzlab.ac.cn (Y. Lu), duguizhi@scu.edu.cn (G. Du).
[1] These authors contributed equally to this work.

https://doi.org/10.1016/j.ijbiomac.2024.132892
Received 15 November 2023; Received in revised form 21 May 2024; Accepted 2 June 2024
Available online 13 June 2024

excitability. TASK channels are expressed widely, including in carotid body type I cells [1], pulmonary arterial smooth muscle cells [2] and renal arteries [3], and have roles in respiratory chemosensation, the mechanism by which the brain regulates breathing in response to changes in CO_2/H^+. In addition, small amounts are expressed in peripheral tissues, such as pancreas and small intestine [4], where a steady-state alkaline environment is maintained and is critical for enzyme function. Disruption of TASK channels has been implicated in several human disorders [5]. For example, missense mutation or reduced expression of TASK-1 has been identified in patients with pulmonary hypertension [6,7], where loss of this channel is expected to depolarize smooth muscle resting membrane potential which likely favors muscle contraction and hypertension. Overexpression of TASK-3 has been reported in a number of human carcinomas such as breast, lung, colon, and metastatic prostate cancers [8], which may increase resistance to hypoxia in cancer cells with acid-base disturbance [9]. TASK variants are associated with hyperaldosteronism and hypertension [10], causing metabolic alkalosis. Missense mutation in the KCNK9 gene encoding TASK-3 causes KCNK9 imprinting syndrome, a rare genetic disorder characterized by dysmorphic facial features, intellectual disability and hypotonia [11]. Electrophysiological studies revealed that KCNK9 variants associated with imprinting syndrome display decreased channel sensitivity to extracellular pH as well modulation by Gq signaling [11]. These pathophysiologies underscore the need to better understand the molecular mechanisms underlying pH-gating of wild type (WT) or disease-associated TASK channels and to develop potential targeted therapeutic strategies for management of those disorders.

The pH-response profiles of TASK-1 and TASK-3 are similar; currents are maximal at pH ~8–9 but become progressively inhibited as the pH drops. In addition, TASK-3 shares >50 % homology with TASK-1 at the amino acid level [12]. However, these TASK subunits have different pH sensitivities; the p*K*a of TASK-1 is ~7.2–7.5 whereas that of TASK-3 is ~6.0–6.7 [12]. A pore-neighboring, titratable histidine residue, H98, plays a key role in pH sensing in TASK-1 and TASK-3 [13,14]. Recently, it was reported that residues D204, Q77 and Q209 can be proton sensors for mouse or human TASK-1 [15,16]. Mutation of D204, Q77 or Q209 largely abolishes the acidic pH sensitivity but still preserves the alkaline pH sensitivity of the TASK-1 channel. Moreover, these three amino acids are highly conserved among pH-sensitive TASK channels. However, little is known regarding the interactions between the essential pH sensor H98 and these more recently identified pH-sensitive residues remote from H98. Nor is it known whether other candidate pH sensors are present in the TASK-3 channel, which could further tune the pH sensitivity of H98 in both acidic and alkaline extracellular milieux.

The structural and mechanistic basis for TASK-3 pH-gating remains unknown. Recent work on another pH-sensitive K2P channel called TWIK-1 showed that under acidic conditions, protonation of extracellular H122 caused the residue to flip up and close the top of the selectivity filter by displacing the helical cap which blocks extracellular ion access and opens gaps for lipid block of the intracellular cavity [17]. The proton-sensor histidine residue (H122) of TWIK-1 is conserved and is the counterpart of H98 in the TASK subfamily. Whether the conformational changes of TASK channels by pH-gating are similar to those of TWIK-1 remains unknown. Here, we used a combined experimental-computational approach, as described in previous studies [18–22], to identify intermolecular interactions between the key pH sensor H98 and other potentially important pH-sensing residues by molecular modeling and voltage-clamp, and reveal a new pH-gating mechanism by molecular dynamics (MD) simulations.

2. Materials and methods

2.1. Molecular modeling

The closed conformation homology model was generated using the online sever SWISS-MODEL (https://swissmodel.expasy.org/), employing the human TASK-1 crystal structure (PDB ID: 6RV2, 3.0 Å) as a template due to its highest homology identity (72.6 %) among the reported structures [16]. The "user template" mode was utilized for generating the homology model, resulting in a single model. The model's quality was assessed using QMEANDisCos (0.74 ± 0.05) [23]. In comparison with the model generated from Alphafold, aside from the flexible C-terminus, which appears as a large loop, the rest structure closely resembles the model generated on SWISS-MODEL, with and RMSD of 0.335 (212 to 212 atoms, aligned in PyMol). For the open conformation homology model (data not shown), the mouse TASK-2 cryo-EM structure (PDB ID: 6WM0, 3.5 Å) served as the template, with a homology identity of 29.08 % [24]. The QMEANDisCos score for the open model is 0.62 ± 0.05.

Hydrogen bond formation in the mTASK-3 homology model was assessed based on criteria including length (≤ 3.5 Å), angle (≥ 120°) and atomic type, where donor atoms (-FH, -NH, or -OH) form pairs with acceptor atoms (F, N, or O).

2.2. Molecular biology and cell culture

WT and mutant DNA sequences of the mTASK-3 channel were cloned into pCDNA3.0 vector with fused EGFP as a reporter. The mTASK-3 constructs were fully confirmed by DNA sequencing.

HEK293T cells were cultured in DMEM supplemented with 10 % FBS. Cells were transfected with WT or mutant mTASK-3 using PolyJet™ (SignaGen) according to the manufacturer's instructions. Cells were plated onto poly-L-lysine (Sigma-Aldrich) -coated coverslips treated after 12–16 h of transfection. Individual and isolated cells expressing green fluorescence were selected for recording.

2.3. Electrophysiology

Whole-cell recordings were performed at room temperature (21–24 °C) using a MultiClamp 700B amplifier and a Digidata 1440A (Molecular Devices, San Jose, CA). Micropipettes were made from borosilicate glass (B150-86-10; Sutter Instrument, Novato, CA) with 4–6 MΩ resistances. The bath solution contained (in mM): 130 NaCl (or *N*-methyl-D-glucamine, NMDG), 3 KCl, 2 $MgCl_2$, 2 $CaCl_2$, 10 HEPES, and 10 glucose, with pH adjusted using NaOH or HCl to 9.0, 8.4, 7.3, 5.9 and 5.0. Internal solution consisted of (in mM):120 KCH_3SO_3, 4 NaCl, 1 $MgCl_2$, 0.5 $CaCl_2$, 10 HEPES, 10 EGTA, 3 Mg-ATP, and 0.3 GTP-Tris, pH 7.2. The total concentration of Na^+ or $NMDG^+$ and K^+ in the external solutions is 133 mM. Bath solutions with different external K^+ concentrations were obtained by exchanges of equimolar K^+ and Na^+. Voltage commands were applied and currents recorded using pClamp software (Molecular Devices). Cells were held at −60 mV, and depolarizing ramps (0.2 V/s, from −130 to +20 mV) were applied at 5 s intervals. Data were analyzed with pCLAMP 10.6 (Molecular Devices) and Prism 9 (GraphPad Software) software.

2.4. Molecular dynamics simulations and calculation of $pK_{1/2}$ values of titratable amino acid

A model membrane in a periodic boundary condition box with water molecules and ions was generated on the online server CHARMM-GUI (https://charmm-gui.org/) [25]. The DOPC homology bilayer membrane was specifically generated using CHARMM-GUI. Throughout the MD simulations, the lipid force field model employed was lipid17.

Molecular dynamics (MD) simulations, with a time of 500 ns, were carried out using Amber (version 2022). AMBER-ff19SB force field was used to describe the protein and TIP3P was used for water molecules. Geometry optimization was subsequently performed. The temperature was maintained at 310 K using Langevin dynamics with a damping coefficient of 1 ps^{-1}, while the pressure was fixed at 1 atm by the Langevin piston method. Each simulation was conducted with a time step of 2 fs. The protonation states of the titratable residues during MD simulation

were determined with a default pH of 7.0 according to CHARMM-GUI recommendations. For the WT, residue H98 was assigned the protonation state HIE, while residues E31 and D204 were in the deprotonated state. For the double mutant H98K + S31E, residue K98 was protonated, and residues E30, E31 and D204 were deprotonated. For the double mutant H98N + S31E, residues E30, E31 and D204 were deprotonated. Each model, including the WT and the mutants H98K + S31E and H98N + S31E, underwent three separate MD simulations, with each simulation lasting 500 ns.

The root mean square deviation (RMSD) and distances between hydrogen bonds were computed for both WT and the mutants H98K + S31E and H98N + S31E.

Local pH conditions within the protein can influence the interactions by altering the protonation states of ionizable residues [26]. In this study, to assess the protonation of residues E30 and K79, we determined the predicted p$K_{1/2}$ values using the H++ online server (http://newbiophysics.cs.vt.edu/H++/index.php), following previously described methods [27]. The p$K_{1/2}$ results are based on the initial homology model, with a pH setting of 7.0 for the protonation calculations.

2.5. Statistical analysis

Results are presented as mean ± SEM. One-way analysis of variance (ANOVA) with Dunnett's multiple post hoc test as appropriate was used to determine significant differences. Statistical significance was assumed if $P < 0.05$ in a two-tailed analysis.

3. Results

3.1. Homology modeling and intermolecular interactions of pH-sensing residues in mTASK-3 channels

To gain a better comprehension of the proton-gating process, we generated a homology model of the mouse TASK-3 (mTASK-3) channel by using the human TASK-1 (PDB ID: 6RV2) structure as a template. As shown in Fig. 1A, mTASK-3 is a homodimer, consisting of four transmembrane helices (M1-M4), two extracellular caps (EC1 and EC2) and two inner pore domains (P1 and P2). The transmembrane helices and extracellular caps form a scaffold that supports and stabilizes the inner pore domains. The inner pore domains include the selectivity filters (SF1 and SF2) and helices (P1-H1 and P2-H2) suspended like a cradle on the scaffold. The inner pore domains and the scaffold are connected by loops (P1M2-L and P2M4-L). The suspension point of this cradle structure is located in the extracellular entrance, and residues E30, S31, E34 and K79 are the key amino acid residues responsible for formation of the suspension structure. Our model suggests that residues E30 and S31 on the top of M1; E34 on EC1; Q77, W78 and K79 on the loop between EC2 and P1-H1; G102 and T103 on P1M2-L; K107 on M2; D204 adjacent to SF2; and Q209 on P2M4-L mediate the interactions between the pore structures and the scaffold (Fig. 1B). In the WT mTASK-3 model (Fig. 1C), three hydrogen bonds (H-bonds) are formed between $E30^A$ - $G102^B$ and $E30^A$ - $T103^B$, one between $D204^A$ - $K107^B$, another between $S31^A$ - $W78^B$, two between $E34^A$ - $Q77^B$ and $E34^A$ - $W78^B$, and one

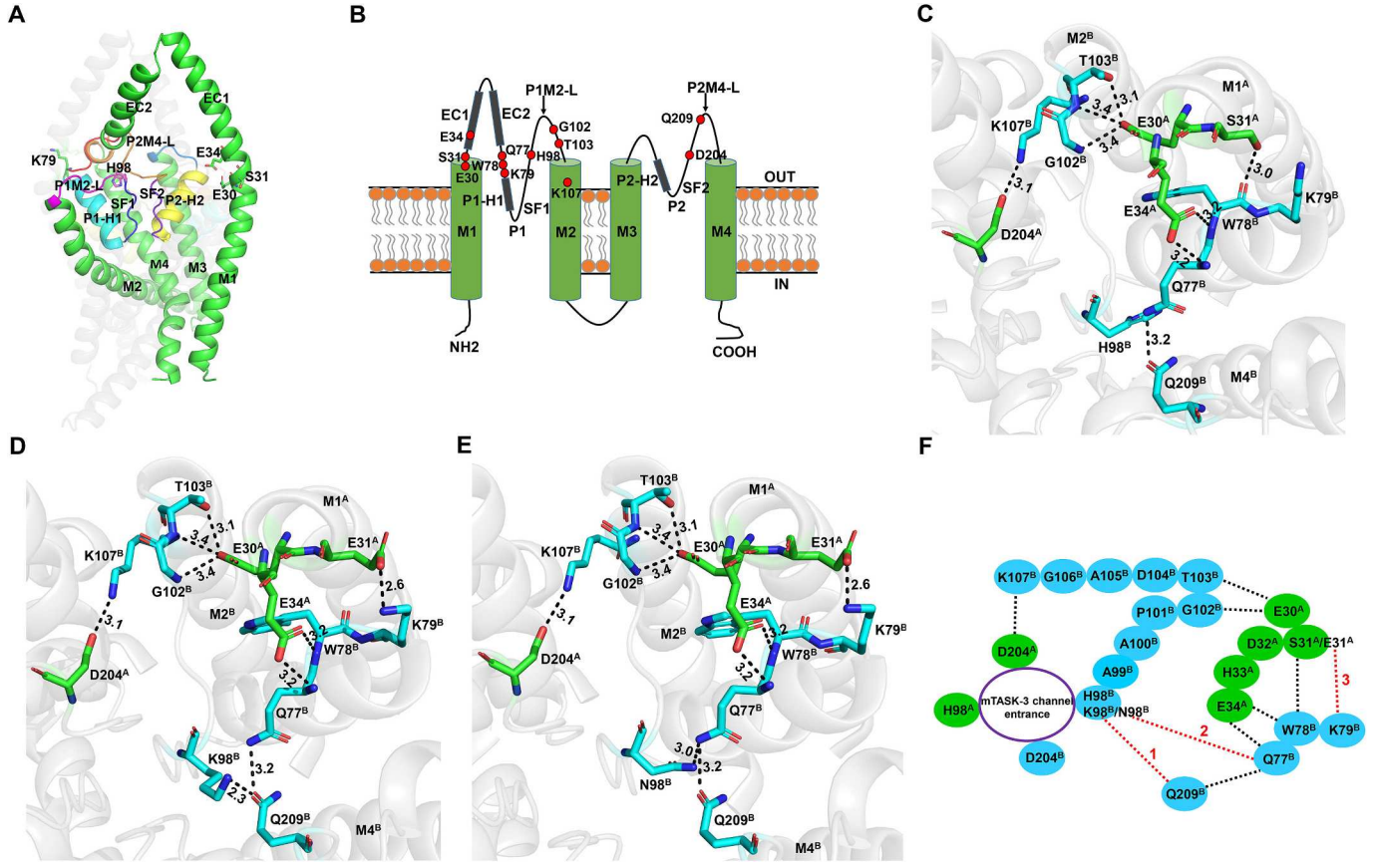

Fig. 1. The overall structure and the interaction network between the scaffold and inner pore domain from the homology model of the mTASK-3 channel. (A) mTASK-3 is shown as a ribbon diagram. The transmembrane helices M1-M4, EC1 and EC2 are colored green; P1-H1, SF1 and P1M2-L are shown in cyan, blue and magenta, respectively; P2-H2, SF2 and P2M4-L are shown in yellow, purple and orange, respectively. Residues E30, S31, E34, K79 and H98 are shown as sticks and labeled. (B) Membrane topology of the mTASK-3 channel showing essential residues in M1-M4, EC1, EC2, P1, P1-H1, SF1, P1M2-L, P2, P2-H2, SF2, and P2M4-L. OUT and IN indicate the extracellular and intracellular compartments, respectively. (C) Hydrogen-bond network in wild type mTASK-3. (D) Hydrogen-bond network in mutant H98K + S31E. (E) Hydrogen-bond network in mutant H98N + S31E. (F) H-bond networks link S31 with the pore entrance residues H98 and D204 in WT mTASK-3 and the mutants H98K/H98N + S31E. H-bonds are indicated by black dashes in WT mTASK-3 and red ones in mutants H98K/N + S31E.

between $Q77^B$ - $Q209^B$ (The superscript A/B indicates that the residue is in chain A or B).

In our model, those H-bonds constitute a large hydrogen-bonding network which can be divided into two parts: one is mediated by residues E30, G102, T103, K107 and D204 and the other by residues S31, W78, E34, Q77 and Q209. This hydrogen-bonding network connects the pore structures and scaffold. Our model identified external residues E30, E34 and S31 (especially E30 and S31) as putative suspension points and essential to the suspension system. Based on this model, we speculated that E30 and S31 (adjacent to E30 and interacting with W78) can remotely fine tune H98 via the hydrogen-bonding network (Fig. 1C). To verify this hypothesis, we built the double mutant models H98K + S31E (Fig. 1D), H98N + S31E (Fig. 1E) and H98N + E30A (Fig. S1, A). Compared to WT mTASK-3, in these two double mutants (K98/N98 + E31), a H-bond is formed between $E31^A$ and $K79^B$. Also, additional H-bond is formed between $K98^B$ and $Q209^B$ in H98K + S31E, or between $N98^B$ and $Q77^B$ in H98N + S31E, thereby further stabilizing the SF region. For clarity and comparative purposes, the H-bond networks are schematized in Fig. 1F, which shows S31 linking with the pore entrance residues H98 and D204 in WT mTASK-3, or the mutant residues H98K/N + S31E. Compared with WT mTASK-3, the combined mutation of E30 and H98 would lead to loss of the H-bonds between $A30^A$ and $G102^B$ and $T103^B$ (Fig. S1, A).

To functionally evaluate our hydrogen-bonding network model of TASK channel modulation, we mutated the predicted essential residues of the hydrogen-bonding network and conducted electrophysiological recording experiments to examine a possible remote fine-tuning effect on the pH-sensor H98 of the TASK-3 channel, as described next.

3.2. Double mutations involving H98 in combination with remote essential residue S31 in the hydrogen-bonding network show a fine-tuning effect on the pH sensitivity of the mTASK-3 channel

We transfected HEK293T cells with WT or mutant mTASK-3 channel constructs and tested the transfectants for responsiveness to changes in extracellular pH in physiological K^+ bath solutions (Fig. 2). As expected, WT TASK-3 exhibited a characteristic pH response profile; channels were maximally active at an alkaline bath pH of 9.0 and fully inhibited at pH 5.0, and show graded degrees of inhibition at intermediate pH values spanning this range (Fig. 2A). Importantly, all pH responses were reversible. We then systematically mutated residues predicted by our model as being important elements of TASK-3's hydrogen-bonding network and reassessed the pH sensitivity of HEK cells expressing these channel mutants. Single point mutations at E30 (Fig. S1, B), S31 or K79 resulted in a pH sensitivity indistinguishable from that of WT channels. It should be noted that E30A decreased peak current to ~1/3 that of WT (Fig. S1, B), whereas mutation of S31, K79 and H98 had negligible effects on channel conductance. As previously reported, the mutant channels H98K and H98N displayed reduced proton sensitivity (Fig. 2B and C). Importantly, we also found that expression of H98N together with mutations in other pH-sensing residues further decreased channel conductance and pH sensitivity. For example, the expression of H98N, together with E30A (Fig. S1, C), K79A (Fig. 2D) or S31E (Fig. 2F), reduced channel conductance and altered ion selectivity (H98N + E30A), or decreased pH sensitivity (H98N + K79A/S31E). The mutation of H98N + E30A led to a significant shift of the reversal potentials towards more depolarized values in Na^+-based bath solutions under alkaline, neutral or acidic pH conditions. Removal of external Na^+ by $NMDG^+$ resulted in a leftward shift of the reversal potentials at all pHs (-38.1 ± 14 mV vs. -14.8 ± 6.5 mV for pH 8.4, -47.0 ± 10.4 mV vs. -11.9 ± 6.2 mV for pH 7.3, -37.4 ± 10 mV vs. -9.4 ± 8.7 mV for pH 5.9, $n = 6$; Fig. S1, D), indicating a loss of channel properties of mTASK-3 which becomes permeable to Na^+ primarily at acidic pH. Surprisingly, the effect of extracellular pH change on the mutated channel was reversed in double mutants of H98 with S31 (Fig. 2, E and D), which showed a complete blocking effect of inhibition by extracellular acidification (pH 5.9 and 5.0) and a partial blocking effect of activation by extracellular alkalization (pH 9.0 and 8.4).

The changes in ion selectivity of WT mTASK-3 and mutant H98N + S31E were measured at alkaline and acidic pH in Na^+-based solutions under various external K^+ conditions and in $NMDG^+$-based bath solutions (Fig. 3A–G). At normal K^+ concentration (3 mM), the reversal potential for WT was more depolarized at pH 5.9 than at pH 8.4: -45.8 ± 11.5 mV vs. -89.5 ± 2.4 mV, $n = 4$; (Fig. 3A), suggesting that acidification disrupts WT channel selectivity probably by increasing Na^+ permeability. This switch in ion selectivity of the channel by extracellular acidification was also retained in high extracellular K^+ (120 mM) bath solution (Fig. 3B). In contrast, the double mutant H98N + S31E eliminates the dynamic ion selectivity of the channel. At physiological K^+ concentration, upon acidification from 8.4 to 5.9 pH, the reversal potential for the mutant was more hyperpolarized (-53.6 ± 10.5 mV vs. -68.3 ± 8.5 mV, $n = 6$; Fig. 3C), implying the double mutant rescues K^+ selectivity at extracellular acidification and becomes permeable to external Na^+ in response to external alkalization. At high K^+ concentration, the mutant channel displayed altered ion selectivity at both pH 5.9 and pH 8.4 (Fig. 3D). As shown in Fig. 3E, the reversal potentials of both the WT and mutant channels are shifted to more depolarized potentials with increasing extracellular K^+ concentration. The reversal potentials for WT mTASK-3 recorded in pH 5.9 bath solutions with 10 and 30 mM K^+ are also more depolarized than those obtained in pH 8.4 and 7.3. Conversely, the reversal potentials for channels expressing H98N and S31E recorded in pH 8.4 and 7.3 bath solutions with 10 and 30 mM K^+ are still much more depolarized than those in pH 5.9. When extracellular Na^+ was replaced with equimolar $NMDG^+$, the reversal potentials of WT mTASK-3 shifted to the left upon acidification compared with those in Na^+-based solution (-68.1 ± 13.8 mV vs. -45.8 ± 11.5 mV, $n = 6$; Fig. 3F), implying a significant increase in the Na^+ to K^+ relative permeability of the channel at acidic pH. In contrast, the reversal potential of H98N + S31E did not shift at pH 5.9 (-69.5 ± 10.4 mV vs. -66.9 ± 8.6 mV, $n = 9$), but shifted to the left at pH 8.4 (-67.0 ± 12.4 mV vs. -53.6 ± 10.4 mV, n = 9) in $NMDG^+$-based bath solutions compared to those in Na^+-based bath solution (Fig. 3G). This indicates that this mutant exhibits no permeability to Na^+ at acidification and a relatively increased Na^+ to K^+ permeability at alkalization.

The pH inducing 50 % of the maximal current amplitude (pH_{50}) and the percentage inhibition at different pH levels relative to I_{max} were determined for the WT and mutant channels (Fig. 4). The pH titration curves show effects of varying extracellular pH on HEK cells expressing each channel construct (Fig. 4A). Single or double mutations involving site H98 exhibit significant shifts in pH_{50} values compared with WT. The pH_{50} is reduced for H98K, H98N and H98N + K79A mutants (Fig. 4B). These mutations decrease acid responses as reflected in decreases in the degree of inhibition at pH 5.9 and 5.0, but with preserved sensitivity to bath alkalization (pH 8.4 and 9.0) like WT (Fig. 4C). In contrast, double mutation of H98 and the remote residue S31 elevate the channel pH_{50} (7.7 ± 0.2, $n = 11$ for H98K + S31E and 7.7 ± 0.2, n = 6 for H98N + S31E vs. 6.8 ± 0.1, n = 9 for WT, $P < 0.001$), resulting in channels that do not respond to extracellular acidification and are only modestly activated by alkalization. Strikingly, these results show that the pH sensitivity of H98K + S31E and H98N + S31E is opposite to that of WT channels (inhibition at alkalization and activation at acidification) (Fig. 4A), suggesting that residue S31 can remotely fine tune the mTASK-3 pH sensor H98. Furthermore, H98 mutation combined with mutation of the remote residue K79 results in a further reduction in pH sensitivity, as shown by the lower pH_{50} (4.3 ± 0.6, $n = 7$ for H98N + K79A and 5.6 ± 0.2, n = 7 for H98N, $P < 0.001$) and the decreased inhibition degree at pH 8.4, 7.3, and 5.9, compared with H98N, indicating K79 also plays a role in remote fine-tuning of the pH sensor H98.

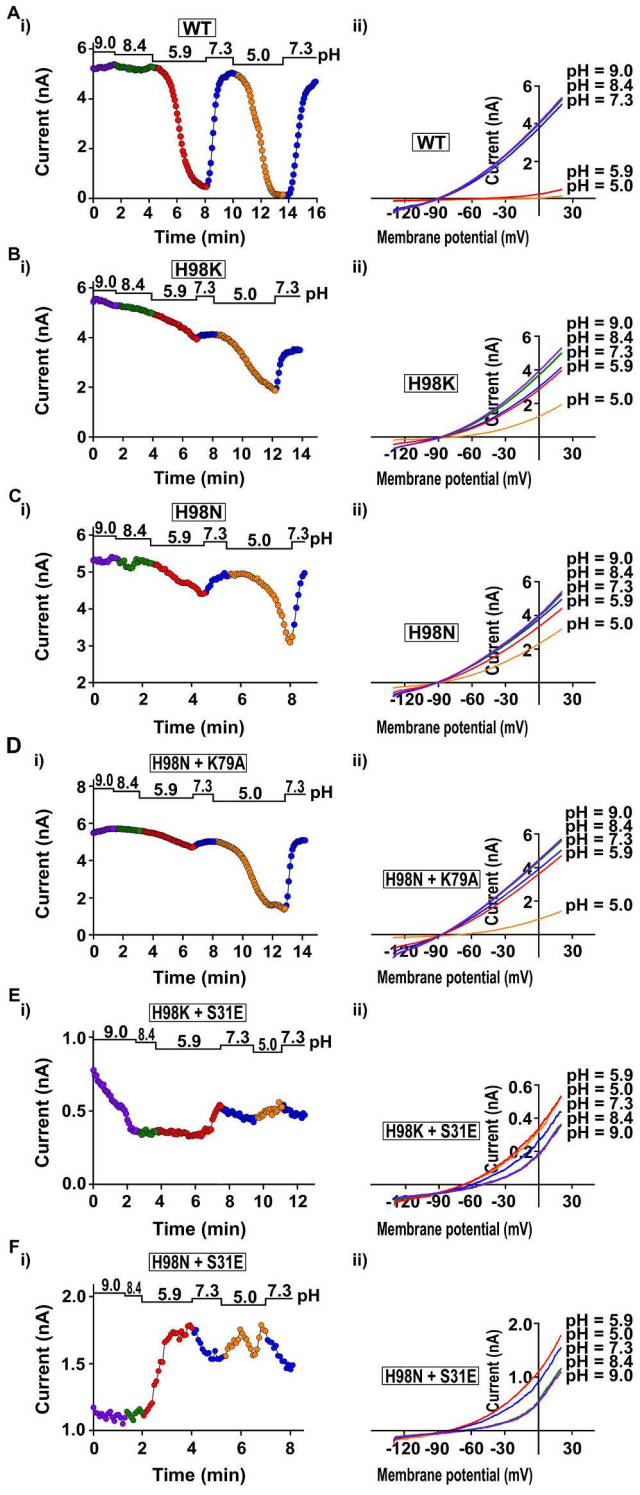

Fig. 2. Sensitivity of WT and mutant mTASK-3 channels to external pH. HEK 293 cells were transfected with WT and mutant constructs. Ramp voltage commands (−130 mV to 20 mV, 0.1 V/s at 0.2 Hz, at a holding potential of −60 mV) were used to elicit currents in response to variations in pH (9.0, 8.4, 5.9, 7.3 and then 5.0) at an intracellular [K^+] of 120 mM throughout. Representative peak current traces recorded in extracellular medium of 130 mM Na^+ and 3 mM K^+ for the WT (A) and mutants H98K (B), H98N (C), H98N + K79A (D), H98K + S31E (E) and H98N + S31E (F). Time series of peak WT mTASK-3 and mutant currents obtained under the indicated conditions (*i*). *I* -V curves of WT mTASK-3 and mutant currents under the indicated conditions (*ii*).

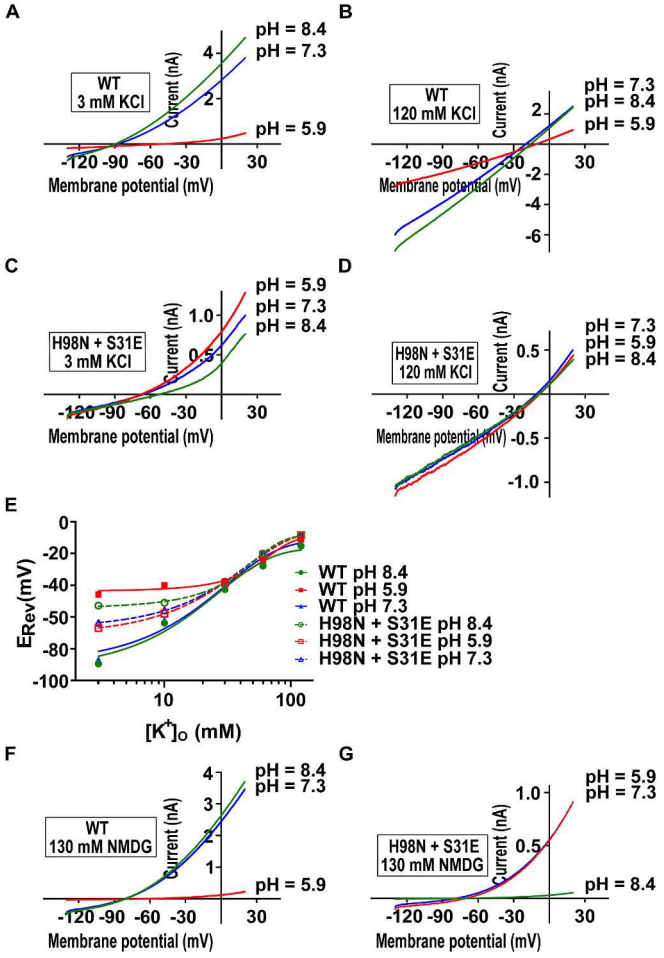

Fig. 3. Selectivity of WT mTASK-3 and mutant H98N + S31E to external pH in Na^+-based solution under normal and high extracellular K^+ conditions, and in $NMDG^+$-based solution. (A–D) Current-voltage relations for WT mTASK-3 and the mutant H98N + S31E in Na^+-based solution at high and low extracellular pH under different external K^+ concentrations (3 mM K^+ and 130 Na^+, and 120 mM K^+ and 13 mM Na^+ for the medium). (E) Reversal potentials of WT mTASK-3 and the mutant H98N + S31E in Na^+-based solution at different extracellular pH (8.4, 5.9 and 7.3) under varying external K^+ concentrations (3, 10, 30, 60 and 120 mM K^+). Extracellular Na^+ was replaced with an equimolar amount of K^+. (F-G) Current-voltage relations for WT mTASK-3 and the mutant H98N + S31E in $NMDG^+$-based solution at high and low extracellular pH (3 mM K^+ and 130 $NMDG^+$).

3.3. Molecular dynamics simulations – combined mutation of H98 with S31 primarily regulates the stability of the pore selective filter and pore loop

Next, we used MD simulations (500 ns, 3 times) to analyze the stability of the suspension structure and interactions between residues of the hydrogen bond network that appears to control the pH sensor H98 of mTASK-3. Considering the limited resolution of the template structure (6RV2) at 3.0 Å with poor water molecule densities, we did not introduce water molecules into the homology model. We found the RMSD values of the central pore structures including the pore selective filter (P-SF) and the pore-Loop (P-Loop) to be significantly affected by the double mutations. Compared to WT, in double mutant H98K + S31E, the average RMSD for three replicas of P-SF increased from 1.94 Å to 2.22 Å, while that of P-Loop decreased from 3.49 Å to 2.88 Å (Fig. 5A). In double mutant H98N + S31E, the average RMSD for three replicas of P-SF decreased from 1.94 Å to 1.48 Å, with no clear difference observed for P-Loop (Fig. 5B). The pore-helix (P—H) region (Fig. 5C) and the external

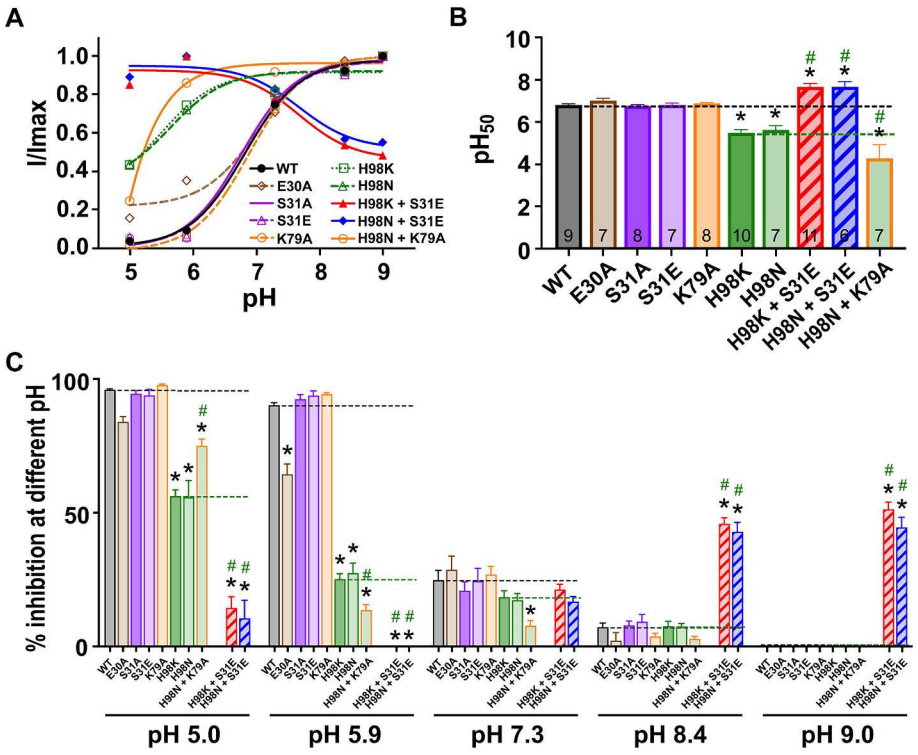

Fig. 4. pH sensitivity of WT mTASK-3 and mutants. (A) pH dose-response curves of WT and mutant channels. *I/I*max = current normalized to that at pH 9.0 for WT, S31E, K79A, H98K, H98N and H98N + K79A, and that at pH 5.9 for H98K + S31E and H98N + S31E. Solid curves are best fits to the Sigmoidal dose-response equation (B). The measured pH_{50} (the pH inducing 50 % of the maximal current amplitude) of WT and mutant channels. The numbers of independent experiments for each channel (n) are indicated as small insets in the respective bars. (C) Percentage inhibition at different pH relative to pH 9.0 for WT, H98K, H98N and H98N + K79A, and relative to pH 5.9 for H98K + S31E and H98N + S31E. *, Statistical significance compared with WT ($P < 0.01$). #, Statistical significance compared with H98K ($P < 0.001$).

scaffold helices M1-M4 (M—Helix) (Fig. 5D) demonstrated RMSD values similar to those of WT. The root mean square fluctuation (RMSF) values for three replicas of WT and double mutant mTASK-3 channels exhibited variation across different regions (Fig. S2). The P-Loop demonstrated the highest average values, whereas the P-SF displayed the smallest. Notably, the fluctuation within the P-SF was higher in H98K + S31E (H98K + $S31E^A$: 1.87 ± 0.06 Å and H98K + $S31E^B$: 2.01 ± 0.14 Å) compared to WT (WT^A: 1.68 ± 0.04 Å and WT^B: 1.87 ± 0.05 Å). Conversely, the fluctuation within P-Loop was more pronounced in H98N + S31E (H98N + $S31E^A$: 2.92 ± 0.12 Å and H98N + $S31E^B$: 3.32 ± 0.18 Å) compared to WT (WT^A: 2.46 ± 0.09 Å and WT^B: 2.89 ± 0.15 Å). Based on the RMSD and RMSF analyses for three replicas of P-SF, P—H, P-Loop and M—helix, it appears that the M—Helix and P—H contribute relatively to maintaining the stability of the entire protein. However, the P-SF and P-Loop regions, crucial for channel selectivity and permeability, exhibit proper flexibility in response to changes in the surrounding environment. This delicate structure enables the external signals to transmit to the pore without inducing drastic global conformational changes in the channel. Therefore, our modeling suggests that double mutation of H98 and S31 could regulate the structural stability of P-SF and P-Loop, which is highly related with the function of this ion channel.

Our model also suggests that in WT, the distance between the side chain hydroxyl of $S31^A$ and the side chain amino group of $K79^B$ remains at ~5 Å throughout the 500 ns of MD simulation (Fig. 5E), suggesting that the H-bond $S31^A$ - $K79^B$ may not be essential for maintaining the suspension system, but could be a potential regulatory site. In contrast, in the H98K + S31E mutant, the distance between the side chain carboxyl of $E31^A$ and the side chain amino group of $K79^B$ was ≤ 3.5 Å for 38 % across the entire 500 ns simulation (distance frequency) (Fig. 5F). Additionally, in the H98N + S31E mutant, this distance was ≤ 3.5 Å for 73.0 % of the 500 ns simulation (Fig. 5G). This supports the finding that the hydrogen bond frequencies between $E31^A$ and $K79^B$ in these mutants were higher compared to WT mTASK-3 (89.6 % for H98N + S31E, 45.9 % for H98K + S31E, and 3.5 % for WT, Fig. S3, A). These results suggest that the H-bond interaction between $E31^A$ and $K79^B$ contributes to the stability of the mutants. Moreover, in the mutants, the side chain carboxyl of $E31^A$ and the side chain amino group of $K79^B$ can form two hydrogen bonds in some frames, resulting in a slightly higher hydrogen bond frequency than the distance frequency (≤ 3.5 Å). Furthermore, the simulations revealed that three H-bonds (one $E30^A$ - $G102^B$ and two $E30^A$ - $T103^B$) were stable in both WT and H98N + S31E channels. However, only the $E30^A$ - $G102^B$ H-bond remained stable in the H98K + S31E mutant (Fig. 5I). The hydrogen bond frequency for $E30^A$ - $G102^B$ or $E30^A$ - $T103^B$ showed no significant differences among the variants (Fig. S3, B and C). The H-bond network consisting of E30, G102, T103, K107, D204, S31, W78, E34, Q77 and Q209 can play an important role in transmitting the external signals to the central pore domain when this ion channel functions. More importantly, the RMSD for three replicas of the pH sensor K98 or N98 in the double mutant H98K+ S31E or H98N + S31E is comparable to that of the pH sensor H98 in WT (1.35 ± 0.01 Å and 1.45 ± 0.01 Å vs. 1.38 ± 0.01 Å) (Fig. 5K). This suggests that substitution of S31 by glutamic acid can influence the ion permeability of this channel primarily through conformational changes in the P-SF and P-Loop regions, rather than solely affecting the sensor residue (H98, K98 and N98, for wild type, double mutant H98K+ S31E and H98N + S31E, respectively).

3.4. Combined mutation of S31 with H98 alters the ionization state of titratable residues E30 and K79 adjacent to S31

The remote fine-tuning effect of residue S31 on the pH sensor H98

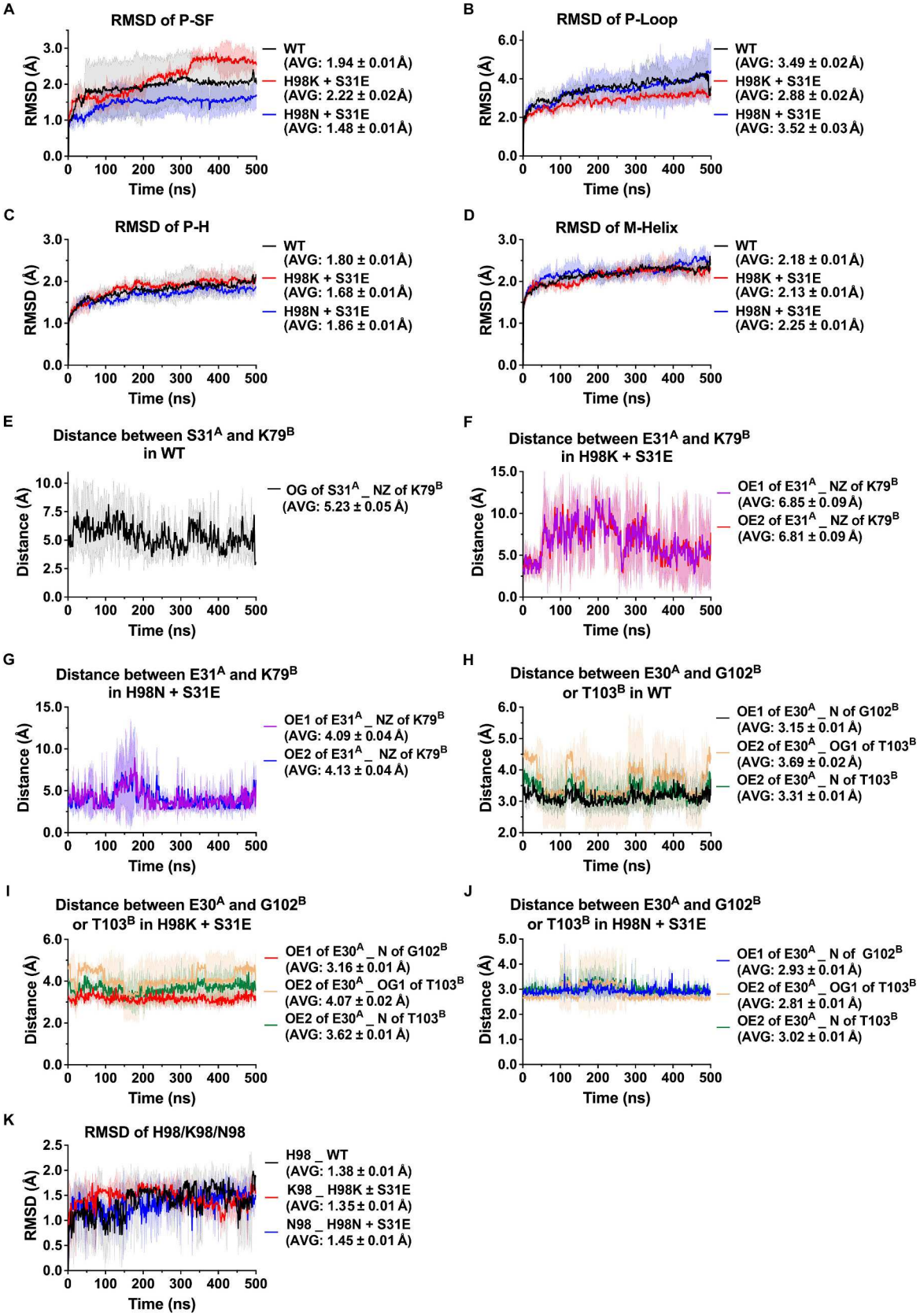

Fig. 5. MD simulations of WT, H98K + S31E and H98N + S31E mutants of the mTASK-3 channel. (A–D) Root mean square deviation (RMSD) calculated for P-SF, P-Loop, P—H and M—Helix regions of the channels. (E) The distance between the hydroxyl oxygen atom (OG) of $S31^{A}$ and the NZ atom of $K79^{B}$ in WT mTASK-3. (F) and (G) Distances between the carboxyl oxygen atom (OE) of $E31^{A}$ and the NZ atom of $K79^{B}$ in double mutants H98K + S31E and H98N + S31E, respectively. (H), (I) and (J) Distances between the OE of $E30^{A}$ and the N atom of the $G102^{B}$ backbone, the OE of $E30^{A}$ and the OG as well as the N atom of the $T103^{B}$ backbone in WT, H98K + S31E and H98N + S31E mutants, respectively. (K) RMSD for H98 in WT and K98 or N98 in H98K + S31E or H98N + S31E.

may be mediated by change of the p$K_{1/2}$ of the residues E30 and K79. To test this hypothesis, we calculated the p$K_{1/2}$ values of those ionizable residues in WT and mutant channels (H98K + S31E and H98N + S31E) using the H++ online server [27]. Subsequently, we estimated the p$K_{1/2}$ values of E30 and K79 for WT and H98K + S31E and H98N + S31E mutants of the mTASK-3 channel (Fig. S4). Consistent with our model's prediction, the proportions-pH curves show a right shift for the double mutants, with increases in p$K_{1/2}$ values of E30 and K79 for H98K + S31E (8.1 and >12 respectively) and H98N + S31E (8.2 and >12 respectively) compared with WT (6.1 and 8.5 respectively). These results indicate that double mutation of H98 and S31 can increase the p$K_{1/2}$ for the essential titratable residues E30 and K79 in the H-bond network. These results suggest that the ionization state of E30 affects the conformational change of N98/K98 as the extracellular pH drops from 9.0 to 5.0, which in turn affects the conductivity of SF of the mutants.

4. Discussion

TASK-3 is a member of the K2P channel family that is sensitive to changes in extracellular pH. Despite identification of many pH-sensing amino acids of TASK-3 such as H98, D204, Q77 and Q209, little is known about the intermolecular interactions between the key pH sensor H98 and the recently described remote residues involved in pH sensing. In addition, mutation of the currently identified pH sensors for TASK channels causes only reduced sensitivity to extracellular acidic pH and a normal response to extracellular alkaline pH rather than complete loss of pH dependence. Nor is it known whether there are other candidate pH sensors present in TASK channels that could remotely tune H98 and influence the response to both lower and higher pH. Using molecular modeling and voltage-clamp, we identified that an H-bond network links H98 with remote titratable residues, including previously reported proton sensors, and that mutation of residue E30, S31 or K79 combined with mutation of H98 can change the conductive properties of the channel, with H98N + E30A causing reduced K^+ conductance and H98N + K79A and H98K/H98N + S31E disrupting pH sensitivity. Surprisingly, mutation of both S31 and H98 nearly completely abolishes the response to extracellular pH and causes loss of ion selectivity from acidification to alkalization. To understand the molecular mechanism underlying the functional loss of pH sensitivity by mutation of S31 coupled with H98, we performed MD simulations and p$K_{1/2}$ calculations and found that these double mutations primarily modulate the flexibility of the P-SF and P-Loop regions in the pore domain, and the H-bond interaction between $E31^A$ and $K79^B$ contributes to the stability of the mutants. The ionization state of E30 and K79 (which are adjacent to and interact with S31) may affect the H-bond network that is an important linkage between external scaffold and inner pore domain. Consequently, changes in the external environment transmit to the pore region through this H-bond network, regulating the pH response of this ion channel. Overall, our findings confirmed that the critical sites can remotely exert fine-tuning effects on the mTASK-3 pH sensor H98 via a hydrogen-bonding network.

H-bond networks play key roles in the stabilization of inter- and intramolecular packing and functions of molecules [28]. In our molecular modeling, we found that a hydrogen-bonding network of mTASK-3, constituted of E30, G102, T103, K107, D204, S31, W78, E34, Q77 and Q209, links the pH sensor H98 with external residue S31. In agreement, the pH sensitivity of mouse or human TASK-1 [15,16] can be affected by mutation of D204, Q77 or Q209, which are among the conserved residues of the hydrogen-bonding network we identified in our mTASK-3 model. In addition to modeling, we confirmed that the essential sites in the network are functionally involved in the pH-sensing of mTASK-3 via remotely tuning H98. Furthermore, based on our MD simulations of WT mTASK-3 and mTASK-3 mutated at H98 and S31, H-bond frequency analyses, coupled with p$K_{1/2}$ estimations of the relevant titratable residues of the network, we further demonstrated the important role of the H-bond network in stabilization of pore structure and modulation of the pH sensor H98 by S31 in the channel. A similar hydrogen-bonding network involved in pH sensing may also exist in other K2P family members, including TASK-2, TWIK, TALK, TREK and TRAAK, because those critical residues are highly conserved among pH-sensitive K2P channels (Fig. S5) and several have been found to be important in pH gating based on functional studies, for example E27 (E28) of TASK-2 [29], E84 of TREK-1 [30] and D230 of TWIK-1 [17]. Taken together, we proposed that the critical residues E30 and K79 in the H-bond network play an important role in remote tuning of pH sensing by S31, and verified that hypothesis by electrophysiology, MD simulations, H-bond frequency analyses and p$K_{1/2}$ calculations of essential residues.

Utilizing homology modeling, we also identified that the hydrogen-bonding network connects the pore and scaffold structures, and residues E30, S31, E34 and K79 (particularly E30 and S31) in the network are essential for the formation of the suspension points that allow SF to be suspended on the scaffold. Consistent with previous reports [31], mutation of E30 in TASK-3 reduces the current amplitude, whereas double mutation of E30 and H98 compromises K^+ selectivity, as evidenced by a shift to more positive reversal potentials whether in Na^+- or $NMDG^+$-based solution (Fig. S1, C and D). As reported before, this glutamate residue (E30) is highly conserved among K2P channels and is presumably involved in gating in all family members [29]. The homologous amino acid in TASK-2 is E27 [29] while in TREK-1 it is E84 [30]. Mutation of the corresponding glutamate site leads to a reduction in current density, possibly via breaking H-bonds between E27 and K107/T108 for TASK-2, or via facilitating a collapse of SF by protonation of extracellular histidine residues for TREK-1. Consistent with those findings, replacing E30 in mTASK-3 with an alanine residue causes a change in ion selectivity, possibly via a similar mechanism in which the H-bonds between $A30^A$ and $G102^B$ and $T103^B$ are broken (Fig. S1, A), implying that the whole hydrogen-bonding network is critical for natural conformational change of the K2P channel pore, and breaking of E30-mediated H-bonds in the network could affect gating of the channel.

As reported for TASK-2 [29], the conserved E30 residue in mTASK-3 is critical for the H-bond network consisting of $E30^A$ - $G102^B$ and $T103^B$ ~ $K107^B$ - $D204^A$ and responsible for maintaining and stabilizing the cradle suspension system. S31, adjacent to E30, connects to the pH-sensing residue H98 by another H-bond network which is composed of $S31^A$ - $W78^B$, $E34^A$ - $Q77^B$, $E34^A$ - $W78^B$ and $Q77^B$ - $Q209^B$ in WT mTASK-3. Neither the E30-involved H-bond network nor the S31-connected H-bond network is broken when in double mutants of S31 with H98. However, the E31-connected H-bond network of the double mutants differs from that of WT due to the additional formation of H-bond in H98K + S31E ($K98^B$ - $Q209^B$) and in H98N + S31E ($N98^B$ - $Q77^B$), coupled with increased H-bond interactions between $E31^A$ and $K79^B$. The additional H-bonds interactions in the double mutants, further strengthen the stability of the cradle suspension system, rendering the pore structure unable to collapse in response to extracellular acidification and difficult to fully activate by alkalization. This result is supported by the identification in MD that double mutation of H98 and S31 markedly improved the structural stability of the P-SF (H98N + S31E, Fig. 5A) and P-Loop (H98K + S31E, Fig. 5B) by a reduction in RMSD, blocking the conformational change of the SF and P-Loop in response to pH changes. Recently, Turney et al. [17] reported both the open conformation (pH 7.4) and the closed conformation (pH 5.5) cryo-EM structure of TWIK-1. A key difference between the open and closed conformations is that the side chain of H122 is flipped from the inside (Fig. S6, A, open conformation) to the extracellular solvent-accessible side of the ion channel (Fig. S6, B, closed conformation). Interestingly, our 500 ns MD simulations showed a similar flip for the side chain of H98 in WT mTASK-3. However, in the double mutants H98K + S31E and H98N + S31E, neither K98 nor N98 displayed this kind of flip, as demonstrated by the corresponding trajectories of H98, K98 and N98 in WT and double mutants (Video S1). The trajectory difference of residue H98/K98/N98 in WT and double mutants helps explain the electrophysiology result, that those double mutants showed

acidic enhancement of current, instead of inhibition.

The H-bond network (E30 is the critical residue in one branch and K79 in the other branch) for the mTASK-3 channel, between the central filter region and the outer helix skeleton, can transmit external changes to the filter region and thus cause changes in the conductive properties of the channel. The S31E mutation alters the local microenvironment of E30 by changing its p$K_{1/2}$, which in turn affects the conformation of the pH sensor K98/N98 by impacting the hydrogen-bonding network, thus affecting the sensor's response properties to extracellular pH. We speculate that the p$K_{1/2}$ of E30 is related to the status of the channel. Specifically, the channel is in the closed state when extracellular pH is close to the p$K_{1/2}$ of E30 (6.1 for WT, 8.1 and 8.2 for H98K + S31E and H98N + S31E), possessing lower permeability to K^+ over Na^+ as demonstrated in our study and reported previously [32,33], and in the open state when the pH is far from the p$K_{1/2}$ of E30, showing more permeability to K^+. The mechanism underlying tuning of the pH sensor by a remote essential residue in the H-bond network in mTASK-3 needs further investigation.

In this study, we evaluated the p$K_{1/2}$ of the ionizable residues E30 and K79 from the H-bond network using the H++ tool. It is important to note that lower-resolution X-ray structures can reduce the accuracy of p*K*a predictions. Our predictions were based on a homology model derived from a low-resolution X-ray structure. However, as with all computational methods, the computed differences are generally more accurate than the absolute values. Consequently, the predicted p$K_{1/2}$ values of E30 and K79 for both wild type and double mutants are expected to reflect accurate trends. Our study used empirical approaches to estimate protein residue p*K*a values from single structures, which do not account for the dynamic nature of proteins. To gain a broader understanding of protein behavior, future studies should consider constant pH simulations, which allow for p*K*a changes over time. Additionally, K2P family proteins have been reported to exhibit various conformations in different structures. Generating multiple homology models would provide a more accurate and comprehensive understanding of these conformations. While the hTASK-1 structure (PDB ID: 6RV2) demonstrates the highest homology identity at 72.6 % among all reported K2P family structures, others exhibit much lower homology identities of < 30 %. Despite potential limitations in using the hTASK-1 structure as a template, it remains a valuable resource for our investigation. Another limitation arises from excluding water molecules in the initial homology model due to the limited resolution of the template structure. However, during the equilibration process of MD simulations, water molecules did naturally flow into the channel permeation pathway, allowing water molecules to move and interact with the channel dynamically, contributing to a more realistic simulation of the channel dynamics. Moreover, due to the lack of high-identity homologous structure in the open state, our study focused solely on the H-bond networks in a homology model of the channel's closed state. Further studies, such as enhancing homology models of the open state to enable advanced simulation analysis of the open state TASK-3 channel, will be essential.

This remote tuning effect by a critical residue in the H-bond network may not be limited to pH sensing in pH-sensitive K2P channels, but could also have a role in sensing of temperature, tension or other environmental signals. This suggests that critical residues in the H-bond network of K2P channels could be potential allosteric regulatory sites for modulating molecule development, where the effect of the molecule would be passed through the P—H to the P-SF region and therefore modulate the ion permeability of the channel.

5. Conclusions

Hydrogen-bonding is critical for selectivity and pH sensing in mTASK-3. E30 and S31 are crucial residues acting as suspension points for maintaining and stabilizing the cradle (inner pore domains) suspension system (scaffold and P-Loops). When the E30-involved branch of the H-bond network is disrupted, the channel shows altered selectivity, leading to an attenuated and shifted current amplitude. However, when the S31/K79-involved branch of the H-bond network is strengthened by additional H-bonds interactions together with an altered ionization state of E30, then the conformational change of the pore, especially the flipping-up rearrangement of residue-98, is restricted, resulting in a loss and reversal of pH sensitivity and ion selectivity. Those structural and corresponding functional alterations suggest that the hydrogen-bonding network is important for maintaining natural gating of mTASK-3, and residues E30 and K79 play critical roles in the S31 remote fine-tuning of the pH-sensor K98/N98 by the network. Moreover, E30 is involved in S31 fine tuning, possibly via change in its p$K_{1/2}$. The neighboring region of S31 might be a potential allosteric regulatory site and a target for the development of new TASK-3 channel-modulating molecules.

Supplementary data to this article can be found online at https://doi.org/10.1016/j.ijbiomac.2024.132892.

CRediT authorship contribution statement

Xueming Fan: Writing – review & editing, Writing – original draft, Investigation, Formal analysis, Data curation, Conceptualization. **Yifei Ye:** Writing – original draft, Formal analysis, Data curation, Conceptualization. **Aakash Saha:** Writing – review & editing, Investigation, Formal analysis, Data curation, Conceptualization. **Li Peng:** Writing – original draft, Investigation, Formal analysis, Data curation, Conceptualization. **Chinmai Pindi:** Writing – review & editing, Data curation, Conceptualization. **Qi Wang:** Writing - review & editing, Conceptualization. **Linghui Yang:** Writing – review & editing, Conceptualization. **Jin Liu:** Writing – review & editing, Conceptualization. **Xiangdong Tang:** Writing – review & editing, Conceptualization. **Giulia Palermo:** Writing – review & editing, Software, Data curation, Conceptualization. **Jiayu Liao:** Writing – review & editing, Conceptualization. **Tingting Xu:** Writing – review & editing, Conceptualization. **Yongzhi Lu:** Writing – review & editing, Writing – original draft, Methodology, Investigation, Formal analysis, Data curation, Conceptualization. **Guizhi Du:** Writing – review & editing, Writing – original draft, Supervision, Project administration, Methodology, Investigation, Funding acquisition, Formal analysis, Data curation, Conceptualization.

Declaration of competing interest

The authors have declared no conflict of interest.

Data availability

All data generated or analyzed during this study are included in the manuscript and supporting files.

Acknowledgements

This work was supported by the National Natural Science Foundation of China (grants 81872801 and 82071557); the Ministry of Science and Technology of the People's Republic of China (grant 2021ZD0201900); the Achievement Transformation Project from West China Hospital (grant HX-H2106139). This material is also based upon work supported by the National Institutes of Health (Grant No. R01GM141329, to GP) and the National Science Foundation (Grant No. CHE- 2144823, to GP). This work also used Expanse at the San Diego Supercomputing Center through allocation MCB160059 from the Advanced Cyberinfrastructure Coordination Ecosystem: Services & Support (ACCESS) program, which is supported by National Science Foundation grants #2138259, #2138286, #2138307, #2137603, and #2138296. Computer time was also provided by the National Energy Research Scientific Computing Center (NERSC) under Grant No M3807.

References

[1] D. Kim, E.J. Cavanaugh, I. Kim, J.L. Carroll, Heteromeric TASK-1/TASK-3 is the major oxygen-sensitive background K+ channel in rat carotid body glomus cells, J. Physiol. 587 (Pt 12) (2009) 2963–2975, https://doi.org/10.1113/jphysiol.2009.171181.

[2] B. Manoury, C. Lamalle, R. Oliveira, J. Reid, A.M. Gurney, Contractile and electrophysiological properties of pulmonary artery smooth muscle are not altered in TASK-1 knockout mice, J. Physiol. 589 (Pt 13) (2011) 3231–3246, https://doi.org/10.1113/jphysiol.2011.206748.

[3] A.A. Shvetsova, V.S. Lazarenko, D.K. Gaynullina, O.S. Tarasova, R. Schubert, TWIK-related acid-sensitive potassium channels (TASK-1) emerge as contributors to tone regulation in renal arteries at alkaline pH, Front. Physiol. 13 (2022) 895863, https://doi.org/10.3389/fphys.2022.895863.

[4] I. Kovács, K. Pocsai, G. Czifra, L. Sarkadi, G. Szucs, Z. Nemes, Z. Rusznák, TASK-3 immunoreactivity shows differential distribution in the human gastrointestinal tract, Virchows Arch. 446 (4) (2005) 402–410, https://doi.org/10.1007/s00428-005-1205-7.

[5] X. Fan, Y. Lu, G. Du, J. Liu, Advances in the understanding of two-pore domain TASK potassium channels and their potential as therapeutic targets, Molecules 27 (23) (2022), https://doi.org/10.3390/molecules27238296.

[6] F. Antigny, A. Hautefort, J. Meloche, M. Belacel-Ouari, B. Manoury, C. Rucker-Martin, C. Péchoux, F. Potus, V. Nadeau, E. Tremblay, G. Ruffenach, A. Bourgeois, P. Dorfmüller, S. Breuils-Bonnet, E. Fadel, B. Ranchoux, P. Jourdon, B. Girerd, D. Montani, S. Provencher, S. Bonnet, G. Simonneau, M. Humbert, F. Perros, Potassium channel subfamily K Member 3 (KCNK3) contributes to the development of pulmonary arterial hypertension, Circulation 133 (14) (2016) 1371–1385, https://doi.org/10.1161/circulationaha.115.020951.

[7] L. Ma, D. Roman-Campos, E.D. Austin, M. Eyries, K.S. Sampson, F. Soubrier, M. Germain, D.A. Trégouët, A. Borczuk, E.B. Rosenzweig, B. Girerd, D. Montani, M. Humbert, J.E. Loyd, R.S. Kass, W.K. Chung, A novel channelopathy in pulmonary arterial hypertension, N. Engl. J. Med. 369 (4) (2013) 351–361, https://doi.org/10.1056/NEJMoa1211097.

[8] L. Pei, O. Wiser, A. Slavin, D. Mu, S. Powers, L.Y. Jan, T. Hoey, Oncogenic potential of TASK3 (Kcnk9) depends on K+ channel function, Proc. Natl. Acad. Sci. U. S. A. 100 (13) (2003) 7803–7807, https://doi.org/10.1073/pnas.1232448100.

[9] N. Comes, A. Serrano-Albarrás, J. Capera, C. Serrano-Novillo, E. Condom, Y.C. S. Ramón, J.C. Ferreres, A. Felipe, Involvement of potassium channels in the progression of cancer to a more malignant phenotype, Biochim. Biophys. Acta 1848 (10 Pt B) (2015) 2477–2492, https://doi.org/10.1016/j.bbamem.2014.12.008.

[10] A. Manichaikul, S.S. Rich, M.A. Allison, N.A. Guagliardo, D.A. Bayliss, R.M. Carey, P.Q. Barrett, KCNK3 variants are associated with hyperaldosteronism and hypertension, Hypertension 68 (2) (2016) 356–364, https://doi.org/10.1161/hypertensionaha.116.07564.

[11] M.A. Cousin, E.L. Veale, N.R. Dsouza, S. Tripathi, R.G. Holden, M. Arelin, G. Beek, M.R. Bekheirnia, J. Beygo, V. Bhambhani, M. Bialer, S. Bigoni, C. Boelman, J. Carmichael, T. Courtin, B. Cogne, I. Dabaj, D. Doummar, L. Fazilleau, A. Ferlini, R.H. Gavrilova, J.M. Graham Jr., T.B. Haack, J. Juusola, S.G. Kant, S. Kayani, B. Keren, P. Ketteler, C. Klöckner, T.T. Koopmann, T.M. Kruisselbrink, A. Kuechler, L. Lambert, X. Latypova, R.R. Lebel, M.S. Leduc, E. Leonardi, A.M. Lewis, W. Liew, K. Machol, S. Mardini, K. McWalter, C. Mignot, J. McLaughlin, A. Murgia, V. Narayanan, C. Nava, S. Neuser, M. Nizon, D. Ognibene, J. Park, K. Platzer, C. Poirsier, M. Radtke, K. Ramsey, C.K. Runke, M.J. Guillen Sacoto, F. Scaglia, M. Shinawi, S. Spranger, E.S. Tan, J. Taylor, A.S. Trentesaux, F. Vairo, R. Willaert, N. Zadeh, R. Urrutia, D. Babovic-Vuksanovic, M.T. Zimmermann, A. Mathie, E. W. Klee, Gain and loss of TASK3 channel function and its regulation by novel variation cause KCNK9 imprinting syndrome, Genome Med. 14 (1) (2022) 62, https://doi.org/10.1186/s13073-022-01064-4.

[12] E.M. Talley, D.A. Bayliss, Modulation of TASK-1 (Kcnk3) and TASK-3 (Kcnk9) potassium channels: volatile anesthetics and neurotransmitters share a molecular site of action, J. Biol. Chem. 277 (20) (2002) 17733–17742, https://doi.org/10.1074/jbc.M200502200.

[13] M.J. Morton, A.D. O'Connell, A. Sivaprasadarao, M. Hunter, Determinants of pH sensing in the two-pore domain K(+) channels TASK-1 and -2, Pflugers Arch. 445 (5) (2003) 577–583, https://doi.org/10.1007/s00424-002-0901-2.

[14] S. Rajan, E. Wischmeyer, G. Xin Liu, R. Preisig-Müller, J. Daut, A. Karschin, C. Derst, TASK-3, a novel tandem pore domain acid-sensitive K+ channel. An extracellular histiding as pH sensor, J. Biol. Chem. 275 (22) (2000) 16650–16657, https://doi.org/10.1074/jbc.M000030200.

[15] K. Yuill, I. Ashmole, P.R. Stanfield, The selectivity filter of the tandem pore potassium channel TASK-1 and its pH-sensitivity and ionic selectivity, Pflugers Arch. 448 (1) (2004) 63–69, https://doi.org/10.1007/s00424-003-1218-5.

[16] K.E.J. Rödström, A.K. Kiper, W. Zhang, S. Rinné, A.C.W. Pike, M. Goldstein, L. J. Conrad, M. Delbeck, M.G. Hahn, H. Meier, M. Platzk, A. Quigley, D. Speedman, L. Shrestha, S.M.M. Mukhopadhyay, N.A. Burgess-Brown, S.J. Tucker, T. Müller, N. Decher, E.P. Carpenter, A lower X-gate in TASK channels traps inhibitors within the vestibule, Nature 582 (7812) (2020) 443–447, https://doi.org/10.1038/s41586-020-2250-8.

[17] T.S. Turney, V. Li, S.G. Brohawn, Structural basis for pH-gating of the K(+) channel TWIK1 at the selectivity filter, Nat. Commun. 13 (1) (2022) 3232, https://doi.org/10.1038/s41467-022-30853-z.

[18] B. Kapur, F. Baldessari, M. Lazaratos, H. Nar, G. Schnapp, A. Giorgetti, A. N. Bondar, Protons taken hostage: dynamic H-bond networks of the pH-sensing GPR68, Comput Struct, Biotechnol. J. 21 (2023) 4370–4384, https://doi.org/10.1016/j.csbj.2023.08.034.

[19] A. Elbahnsi, J. Cowgill, V. Burtscher, L. Wedemann, L. Zeckey, B. Chanda, L. Delemotte, Interplay between VSD, pore, and membrane lipids in electromechanical coupling in HCN channels, Elife 12 (2023), https://doi.org/10.7554/eLife.80303.

[20] C. Domene, L. Darré, V. Oakes, S. Gonzalez-Resines, A potential route of capsaicin to its binding site in the TRPV1 ion channel, J. Chem. Inf. Model. 62 (10) (2022) 2481–2489, https://doi.org/10.1021/acs.jcim.1c01441.

[21] W. Kopec, B.S. Rothberg, B.L. de Groot, Molecular mechanism of a potassium channel gating through activation gate-selectivity filter coupling, Nat. Commun. 10 (1) (2019) 5366, https://doi.org/10.1038/s41467-019-13227-w.

[22] R. Dastvan, A. Rasouli, S. Dehghani-Ghahnaviyeh, S. Gies, E. Tajkhorshid, Proton-driven alternating access in a spinster lipid transporter, Nat. Commun. 13 (1) (2022) 5161, https://doi.org/10.1038/s41467-022-32759-2.

[23] G. Studer, C. Rempfer, A.M. Waterhouse, R. Gumienny, J. Haas, T. Schwede, QMEANDisCo-distance constraints applied on model quality estimation, Bioinformatics 36 (6) (2020) 1765–1771, https://doi.org/10.1093/bioinformatics/btz828.

[24] B. Li, R.A. Rietmeijer, S.G. Brohawn, Structural basis for pH gating of the two-pore domain K(+) channel TASK2, Nature 586 (7829) (2020) 457–462, https://doi.org/10.1038/s41586-020-2770-2.

[25] J. Lee, X. Cheng, J.M. Swails, M.S. Yeom, P.K. Eastman, J.A. Lemkul, S. Wei, J. Buckner, J.C. Jeong, Y. Qi, S. Jo, V.S. Pande, D.A. Case, C.L. Brooks 3rd, A. D. MacKerell Jr., J.B. Klauda, W. Im, CHARMM-GUI input generator for NAMD, GROMACS, AMBER, OpenMM, and CHARMM/OpenMM simulations using the CHARMM36 additive force field, J. Chem. Theory Comput. 12 (1) (2016) 405–413, https://doi.org/10.1021/acs.jctc.5b00935.

[26] K.P. Kilambi, K. Reddy, J.J. Gray, Protein-protein docking with dynamic residue protonation states, PLoS Comput. Biol. 10 (12) (2014) e1004018, https://doi.org/10.1371/journal.pcbi.1004018.

[27] R. Anandakrishnan, B. Aguilar, A.V. Onufriev, H++ 3.0: automating pK prediction and the preparation of biomolecular structures for atomistic molecular modeling and simulations, Nucleic Acids Res. 40 (Web Server issue) (2012) W537–W541, https://doi.org/10.1093/nar/gks375.

[28] C. Guzmán-Afonso, Y.L. Hong, H. Colaux, H. Iijima, A. Saitow, T. Fukumura, Y. Aoyama, S. Motoki, T. Oikawa, T. Yamazaki, K. Yonekura, Y. Nishiyama, Understanding hydrogen-bonding structures of molecular crystals via electron and NMR nanocrystallography, Nat. Commun. 10 (1) (2019) 3537, https://doi.org/10.1038/s41467-019-11469-2.

[29] M.J. Morton, A. Abohamed, A. Sivaprasadarao, M. Hunter, pH sensing in the two-pore domain K+ channel, TASK2, Proc. Natl. Acad. Sci. U. S. A. 102 (44) (2005) 16102–16106, https://doi.org/10.1073/pnas.0506870102.

[30] A. Cohen, Y. Ben-Abu, S. Hen, N. Zilberberg, A novel mechanism for human K2P2.1 channel gating. Facilitation of C-type gating by protonation of extracellular histidine residues, J. Biol. Chem. 283 (28) (2008) 19448–19455, https://doi.org/10.1074/jbc.M801273200.

[31] A. Mathie, E. Al-Moubarak, E.L. Veale, Gating of two pore domain potassium channels, J. Physiol. 588 (Pt 17) (2010) 3149–3156, https://doi.org/10.1113/jphysiol.2010.192344.

[32] L. Ma, X. Zhang, M. Zhou, H. Chen, Acid-sensitive TWIK and TASK two-pore domain potassium channels change ion selectivity and become permeable to sodium in extracellular acidification, J. Biol. Chem. 287 (44) (2012) 37145–37153, https://doi.org/10.1074/jbc.M112.398164.

[33] L. Zúñiga, V. Márquez, F.D. González-Nilo, C. Chipot, L.P. Cid, F.V. Sepúlveda, M. I. Niemeyer, Gating of a pH-sensitive K(2P) potassium channel by an electrostatic effect of basic sensor residues on the selectivity filter, PLoS One 6 (1) (2011) e16141, https://doi.org/10.1371/journal.pone.0016141.